Volume 44 | Number 26 | 14 July 2015 | Pages 11673–12012

Dalton Transactions

An international journal of inorganic chemistry

www.rsc.org/dalton

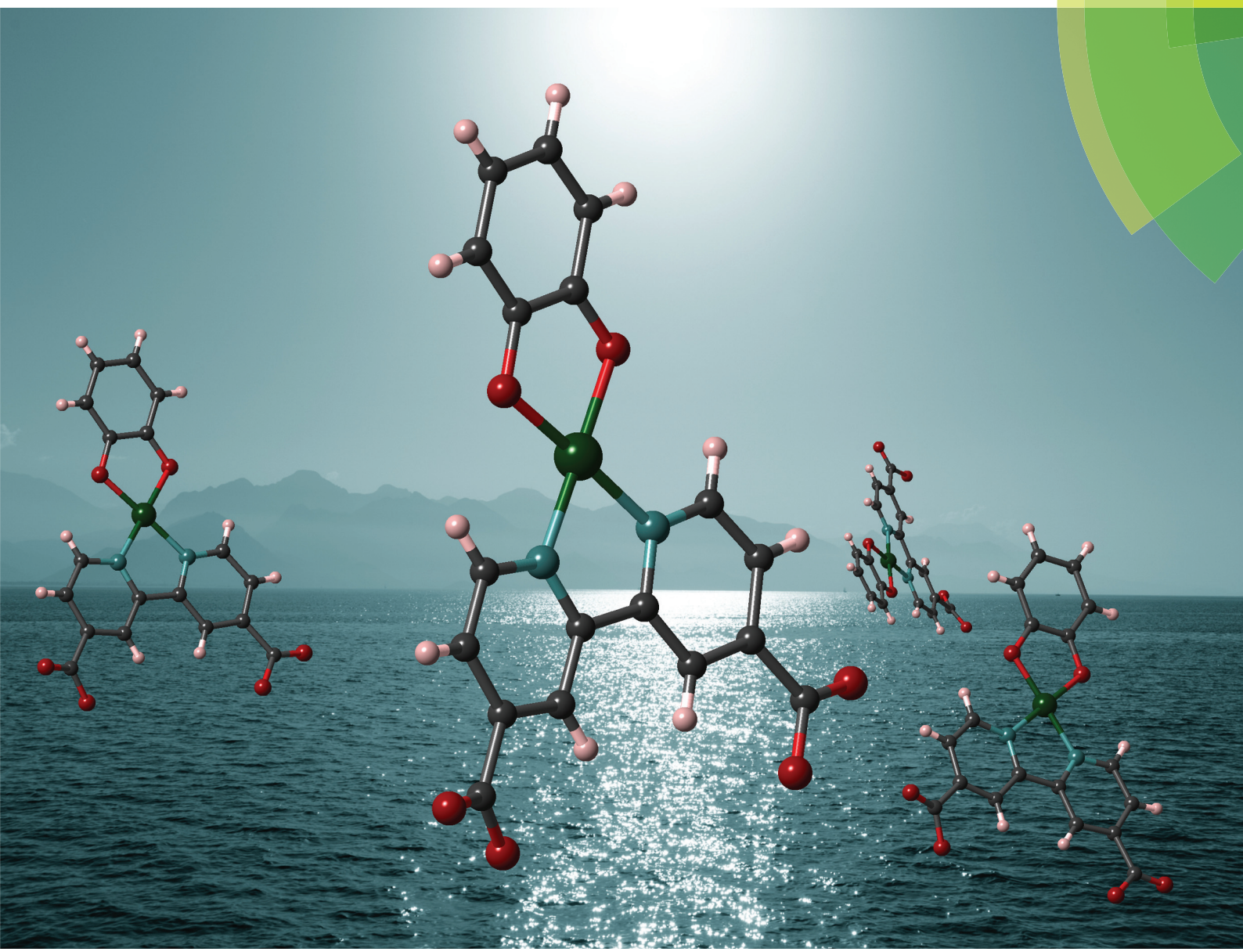

ISSN 1477-9226

ROYAL SOCIETY OF CHEMISTRY

PAPER

Carlos Serpa, Julia A. Weinstein *et al.*

Exploring excited states of Pt(II) diimine catecholates for photoinduced charge separation

Dalton Transactions

PAPER

View Article Online
View Journal | View Issue

Cite this: *Dalton Trans.*, 2015, **44**, 11705

Exploring excited states of Pt(II) diimine catecholates for photoinduced charge separation†

Paul A. Scattergood,[a] Patricia Jesus,[b] Harry Adams,[a] Milan Delor,[a] Igor V. Sazanovich,[a,c] Hugh D. Burrows,[b] Carlos Serpa*[b] and Julia A. Weinstein*[a]

The intense absorption in the red part of the visible range, and the presence of a lowest charge-transfer excited state, render Platinum(II) diimine catecholates potentially promising candidates for light-driven applications. Here, we test their potential as sensitisers in dye-sensitised solar cells and apply, for the first time, the sensitive method of photoacoustic calorimetry (PAC) to determine the efficiency of electron injection in the semiconductor from a photoexcited Pt(II) complex. Pt(II) catecholates containing 2,2′-bipyridine-4,4′-di-carboxylic acid (dcbpy) have been prepared from their parent iso-propyl ester derivatives, complexes of 2,2′-bipyridine-4,4′-di-C(O)O^{i}Pr, (COO^{i}Pr)$_2$bpy, and their photophysical and electrochemical properties studied. Modifying diimine Pt(II) catecholates with carboxylic acid functionality has allowed for the anchoring of these complexes to thin film TiO_2, where steric bulk of the complexes (3,5-di^{t}Bu-catechol *vs.* catechol) has been found to significantly influence the extent of monolayer surface coverage. Dye-sensitised solar cells using Pt(dcbpy)(^{t}Bu$_2$Cat), **1a**, and Pt(dcbpy)(pCat), **2a**, as sensitisers, have been assembled, and photovoltaic measurements performed. The observed low, 0.02–0.07%, device efficiency of such DSSCs is attributed at least in part to the short excited state lifetime of the sensitisers, inherent to this class of complexes. The lifetime of the charge-transfer ML/LLCT excited state in Pt((COO^{i}Pr)$_2$bpy)(3,5-di-^{t}Bu-catechol) was determined as 250 ps by picosecond time-resolved infrared spectroscopy, TRIR. The measured increase in device efficiency for **2a** over **1a** is consistent with a similar increase in the quantum yield of charge separation (where the complex acts as a donor and the semiconductor as an acceptor) determined by PAC, and is also proportional to the increased surface loading achieved with **2a**. It is concluded that the relative efficiency of devices sensitised with these particular Pt(II) species is governed by the degree of surface coverage. Overall, this work demonstrates the use of Pt(diimine)(catecholate) complexes as potential photosensitizers in solar cells, and the first application of photoacoustic calorimetry to Pt(II) complexes in general.

Received 11th November 2014,
Accepted 22nd January 2015

DOI: 10.1039/c4dt03466j

www.rsc.org/dalton

Introduction

Catechol ligands, members of the dioxolene family, have been extensively utilised within the coordination chemistry of various metal ions such as Ru(II),[1–8] Os(II)[4,9,10] and Re(I).[11–13] The most attractive feature of catechol ligands is their rich electrochemistry, with facile and reversible oxidation to semiquinone and quinone forms, together with the strong interplay between catechol and metal-based orbitals frequently resulting in transition metal complexes which display 'non-innocent' behaviour.[14,15] Whilst transition metal catecholates have been widely studied, Pt(II) catecholate chemistry has been rather less explored.[16–25] Previously reported Pt(II) catecholates commonly feature α,α′-diimines such as substituted bipyridines or phenanthrolines, in conjunction with simple dioxolenes, for example pyrocatechol, 3,5-di-*tert*-butyl catechol or 4-*tert*-butyl catechol. These Pt(II)-centred complexes are characterised by the broad, moderately intense, low-energy electronic absorption, being predominantly of a ligand-to-ligand charge transfer nature (LL'CT).[16,17] Previous investigations have shown the aforementioned electronic transition to involve a HOMO which is primarily catechol-based and a diimine localised LUMO, with ligand substitution having a profound effect upon the electronic and photophysical properties of the complex as a whole.[16,21] Catechol ligands have also been utilised to move the lowest energy electronic absorption band of metal complexes into the strategically important near infra-red (NIR)

[a]*Department of Chemistry, University of Sheffield, Sheffield, S3 7HF, UK. E-mail: Julia.Weinstein@sheffield.ac.uk*
[b]*Centro de Química de Coimbra and Chemistry Department, University of Coimbra, P3004-535 Coimbra, Portugal. E-mail: serpasoa@ci.uc.pt*
[c]*Laser for Science Facility, Rutherford Appleton Laboratory, Harwell Science and Innovation Campus, Didcot, OX11 0QX, UK*
†Electronic supplementary information (ESI) available. CCDC 1028955 and 1028956. For ESI and crystallographic data in CIF or other electronic format see DOI: 10.1039/c4dt03466j

region, with the first oxidation potential being typically between −0.2 and +0.2 V *vs.* Fc/Fc^+.

The tuneable nature of both the photophysical and electrochemical properties of Pt(II) catecholates makes them potential candidates for use within inorganic dye-sensitised solar cells (DSSC's). These photoelectrochemical devices are centred around a light absorbing 'dye' molecule anchored to a thin film semi-conductor surface, commonly TiO_2.[26,27] The operational principle of these photovoltaic cells involves the injection of electrons from the photo-excited dye into the conduction band of TiO_2, thereby producing electrical current, with the oxidised dye being regenerated through electron transfer from a redox electrolyte, commonly I_2/I_3^-. The ability to control and fine tune the electronic properties of the dye is of great importance in ensuring efficient electron injection; in the close matching of electrochemical potentials with those of the redox electrolyte and in tailoring the optical absorbance to cover as much of the solar emission spectrum as possible – particularly the NIR region. Whilst substituted polypyridyl-containing Ru(II) complexes have dominated DSSC research to date, a limited range of Pt(II)-centred systems have been explored. For example, previous reports[28–30] introduce a range of diimine Pt(II) dithiolates, with these complexes being anchored onto TiO_2 surfaces through the bipyridine ligands appended with carboxylic acid functionality. These studies take advantage of the easily tuneable Mixed Metal–Ligand-to-Ligand charge transfer (MMLL'CT') transition, with the complexes being subsequently incorporated in DSSCs to give overall device efficiencies (η) typically between 0.1–1.1%. Another report[31] describes a range of terpyridine-containing alkynyl-based Pt(II) sensitisers. These systems were found to exhibit intense optical absorption in the visible region and relatively long-lived charge transfer excited states, with overall device efficiencies reaching $\eta \approx 3.6\%$.

To the best of our knowledge, the potential of Pt(II) catecholates to function as sensitisers within DSSCs remains unexplored. Here, we introduce two new catecholate-based sensitising dyes and investigate their electrochemical and photophysical properties. The uptake of these species onto TiO_2 is evaluated, together with an assessment of their suitability as sensitisers through incorporation within DSSCs and the analysis of current–voltage data.

Electron injection from the dye in its excited electronic state into the conduction band of TiO_2 with the formation of a charge-separated state between the oxidised dye and the electron within the conduction band of the semiconductor is one of the most important processes in DSSCs.[32] The parameter of particular importance is the quantum yield of electron injection, yet it is the quantity which is the most difficult to determine directly. This value is often estimated from the initial amplitude of fast transient absorption signals;[29,33] or determined in absolute terms through the kinetics of the dye emission component quenched by electron injection process,[34,35] assuming that electron injection competes only with the decay of the excited state. We employ here an alternative approach, which allows one to directly determine the yields of injection – namely, photoacoustic calorimetry (PAC).[36,37] This calorimetric technique monitors the photo-induced pressure waves that result from heat deposition processes. Fast piezoelectric transducers are used to evaluate the magnitude of the detected pressure waves which depend upon the non-radiative processes occurring after light absorption, and on the thermoelastic properties of the materials under study. From the relation between the energy absorbed and the heat released the quantum yields of non-radiative processes can be obtained. In the present application, PAC is used for the detection of pressure waves generated upon conversion of excitation energy into heat as the photoexcited dye injects an electron into the conduction band of the semiconductor. Whilst PAC is commonly employed to study the thermodynamics of photoinduced processes in solution,[38] we utilise a front-face set-up to follow electron injection at the TiO_2–dye–solvent interface and to ultimately determine the quantum yield of electron injection. Here, the yield of electron injection is estimated by measuring the yield of formation of the long-lived charge-separation between the oxidised sensitizer, and the semiconductor (ϕ_{cs}).

Previously, we have demonstrated a successful use of PAC for determining the energy of the charge separated state (E_{CS}) formed between the oxidised dye and the electron within the conduction band.[36,37] We now report new transition metal complexes which intensely absorb light in the visible region of the spectrum, investigate their photophysical properties, and evaluate their potential as dyes for DSSCs using the advanced PAC technique.

Experimental

cis-$Pt(DMSO)_2Cl_2$ was synthesised following a previously reported procedure.[39]

Synthesis of $(COO^iPr)_2bpy$

2,2′-Bipyridine-4,4′-dicarboxylic acid, hereafter dcbpy, (350 mg, 1.433 mmol) was suspended in $SOCl_2$ (12 ml) and heated to 85 °C for 48 h. The solvent was removed to leave pale yellow solids which were completely purged of excess $SOCl_2$ under a stream of dry nitrogen for a further hour. The thus obtained acyl chloride functionalised intermediate was then re-dissolved in deaerated 1 : 1 (v/v) toluene–^{i}PrOH (25 ml) and heated to 80 °C for 21 h. Removal of the solvent gave pale yellow coloured solids which were subsequently re-dissolved in $CHCl_3$ (75 ml) and washed with 2 × 75 ml saturated aqueous $NaHCO_3$ solution. The aqueous phases were extracted with a further 1 × 30 ml portion of $CHCl_3$. The combined organic layers were washed with 2 × 50 ml H_2O, dried over $MgSO_4$, filtered and the solvent removed to yield the product as an off-white coloured solid. Yield = 379 mg, 81%. ^{1}H NMR ($CDCl_3$, 400 MHz): 1.42 (d, J = 6.28 Hz, 12H), 5.32 (sept, J = 6.28 Hz, 2H), 7.90 (dd, J = 1.32, 4.82 Hz, 2H), 8.86 (d, J = 4.88 Hz, 2H), 8.92 (d, J = 1.12 Hz, 2H). EI-MS: m/z = 328 (M^+, 34%), 269 ($M^+ - O^iPr$, 42%), 242 ($M^+ - COO^iPr$, 100%).

Synthesis of {(COO^{i}Pr)$_2$bpy}PtCl$_2$

2,2′-Bipyridine-4,4′-diisopropylacetate **(COO^{i}Pr)$_2$bpy** (334 mg, 1.017 mmol) and Pt(DMSO)$_2$Cl$_2$ (423 mg, 1.001 mmol) were suspended in deaerated EtOH (40 ml) and heated to 65 °C in the dark for 20 h. The mixture was allowed to cool to room temperature, with the resultant bright orange coloured precipitate being collected by filtration. The solids were washed with EtOH followed by Et$_2$O and dried *in vacuo*. Yield = 519 mg, 87%. ^{1}H NMR (CDCl$_3$, 400 MHz): 1.48 (d, J = 6.28 Hz, 12H), 5.37 (sept, J = 6.28 Hz, 2H), 8.05 (dd, J = 1.72, 6.05 Hz, 2H), 8.57 (d, J = 1.52 Hz, 2H), 9.73 (d, J = 6.00 Hz, 2H). EI-MS: m/z = 594 (M^+, 55%), 508 (M^+ − COO^{i}Pr, 16%), 328 (M^+ − PtCl$_2$, 14%), 242 (M^+ − PtCl$_2$COO^{i}Pr, 100%). Anal. Calc. for $C_{18}H_{20}N_2O_4Cl_2Pt$ (%): C 36.37, H 3.39, N 4.71, Cl 11.93. Found (%): C 36.19, H 3.31, N 4.57, Cl 11.63.

Synthesis of {(COO^{i}Pr)$_2$bpy}Pt(^{t}Bu$_2$Cat) (1)

3,5-Di-*tert*-butyl catechol (93 mg, 0.418 mmol) and ^{t}BuOK (87 mg, 0.775 mmol) were dissolved in dry, deaerated THF (20 ml) and stirred rapidly at room temperature for 45 min. The deep blue coloured solution was then transferred *via* cannula to {(COO^{i}Pr)$_2$bpy}PtCl$_2$ (222 mg, 0.373 mmol) in dry, deaerated THF (20 ml). The resulting reaction mixture was heated to 75 °C in the dark for 48 h. The solvent was removed and the residue purified by column chromatography (SiO$_2$, slow gradient, 0.1% MeOH–DCM to 0.4% MeOH–DCM). After complete removal of all yellow coloured material the product was collected from a deep blue fraction. Removal of the solvent afforded the title complex as a dark blue coloured solid. Yield = 237 mg, 85%. ^{1}H NMR (CDCl$_3$, 400 MHz): 1.32 (s, 9H), 1.46 (d, J = 6.52 Hz, 6H), 1.48 (d, J = 6.56 Hz, 6H), 1.52 (s, 9H), 5.30–5.44 (m, 2H), 6.47 (d, J = 2.08 Hz, 1H), 6.74 (d, J = 2.12 Hz, 1H), 7.96 (dd, J = 1.64, 6.00 Hz, 1H), 8.04 (dd, J = 1.64, 6.00 Hz, 1H), 8.39 (d, J = 1.16 Hz, 1H), 8.47 (d, J = 1.28 Hz, 1H), 9.61 (d, J = 5.96 Hz, 1H), 9.72 (d, J = 5.96 Hz, 1H). MALDI-MS: m/z = 743.2 (M^+).

Synthesis of {(COO^{i}Pr)$_2$bpy}Pt(pCat) (2)

Pyrocatechol (59 mg, 0.535 mmol) and ^{t}BuOK (80 mg, 0.712 mmol) were added to dry, deaerated THF (40 ml) and stirred rapidly at room temperature for 45 min. The mixture was then transferred *via* cannula to ((COO^{i}Pr)$_2$bpy)PtCl$_2$ (250 mg, 0.420 mmol) and heated to 75 °C in the dark for 60 h. (A deep blue-green colour evolved over the first 30 min.) The solvent was removed and the residue purified by column chromatography (SiO$_2$, slow gradient, 0.2% MeOH–DCM to 1.1% MeOH–DCM). After complete removal of all yellow and orange coloured material the product was obtained from a deep blue fraction. Removal of the solvent afforded the title complex as a dark blue solid. Yield = 141 mg, 53%. ^{1}H NMR (CDCl$_3$, 400 MHz): 1.49 (d, J = 6.24 Hz, 12H), 5.32 (sept, J = 6.28 Hz, 2H), 5.79–5.85 (m, 2H), 5.87–5.94 (m, 2H), 7.49 (dd, J = 1.00, 5.64 Hz, 2H), 7.68 (d, J = 1.04 Hz, 2H), 8.70 (d, J = 5.24 Hz, 2H). MALDI-MS: m/z = 631.0 (M^+).

Synthesis of (dcbpy)Pt(^{t}Bu$_2$Cat) (1a)

KOH (98 mg, 1.746 mmol) was dissolved in 1 : 1 (v/v) THF–H$_2$O (16 ml). The solution was deaerated by bubbling argon for 15 min and then transferred *via* cannula to (**1**) (45 mg, 0.060 mmol). The resulting deep blue coloured solution was stirred at room temperature in the dark for 3 days. The reaction mixture was acidified (pH 4) through the dropwise addition of 0.1 M HCl, yielding a fine precipitate which was subsequently collected by centrifugation. Purification was achieved by thorough washing with H$_2$O, DCM and Et$_2$O to leave fine dark blue solids which were dried *in vacuo*. The product was found to be fully soluble in DMF and DMSO only. Yield = 22 mg, 55%. ^{1}H NMR (d$_6$-DMSO, 400 MHz): 1.22 (s, 9H), 1.46 (s, 9H), 6.28 (d, J = 1.92 Hz, 1H), 6.50 (d, J = 2.08 Hz, 1H), 8.12 (dd, J = 1.72, 5.96 Hz, 1H), 8.21 (dd, J = 1.68, 5.88 Hz, 1H), 8.97 – 9.00 (m, 2H), 9.38 – 9.43 (m, 2H), 14.26 (s broad, 2H). MALDI-MS: m/z = 659.4 (M^+).

Synthesis of (dcbpy)Pt(pCat) (2a)

KOH (129 mg, 2.299 mmol) was dissolved in 1 : 1 (v/v) THF–H$_2$O (16 ml) and deaerated through argon bubbling for 15 min. The basic solution was then transferred *via* cannula to (**2**) (45 mg, 0.071 mmol) and stirred at room temperature in the dark for 3 days. The deep red-purple coloured solution was acidified (pH 4) through the dropwise addition of 0.1 M HCl, yielding a fine precipitate which was collected by centrifugation. Purification was effected by thorough washing with H$_2$O, DCM and Et$_2$O. The resultant dark blue coloured solids were dried *in vacuo*. The product was found to be fully soluble only in DMF and DMSO. Yield = 34 mg, 87%. ^{1}H NMR (d$_6$-DMSO, 400 MHz): 6.17–6.24 (m, 2H), 6.43–6.50 (m, 2H), 8.10 (dd, J = 1.60, 5.92 Hz, 2H), 8.87 (d, J = 1.44 Hz, 2H), 9.29 (d, J = 5.92 Hz, 2H), 14.24 (s, broad, 2H). MALDI-MS: m/z = 547.1 (M^+).

General information

All synthetic manipulations were carried out under an atmosphere of argon using standard Schlenk line techniques. Dry solvents were obtained from a Grubbs solvent purification column. Deaeration of solvents was performed through the vigorous bubbling of argon for a period of at least 15 minutes.

NMR spectroscopy. All ^{1}H NMR spectra were recorded on a 400 MHz Bruker Avance 400 spectrometer. Deuterated solvents were purchased from Sigma Aldrich and were of spectroscopic grade. Chemical shifts are reported in ppm and calibrated relative to the residual solvent signal (CDCl$_3$ 7.26 ppm, d$_6$-DMSO 2.50 ppm).

Mass spectrometry. Positive electron ionisation (EI) mass spectra were recorded through the use of a VG AutoSpec magnetic sector instrument. Matrix Assisted Laser Desorption Ionisation (MALDI) mass spectra were obtained from a Bruker Reflex III instrument fitted with a time-of-flight mass analyser, utilising a DCTB matrix.

Elemental analysis. Elemental microanalysis for carbon, hydrogen and nitrogen was performed using a Perkin Elmer

2400 Series II CHNS/O system. Analysis for chlorine was carried out by the 'Schoniger Flask Combustion' technique.

Electrochemistry. Cyclic voltammograms were measured using an Autolab Potentiostat 100 with General Purpose Electrochemical Software (GPES). Analyte solutions were prepared using dry DCM obtained from a Grubbs solvent purification column. Measurements were conducted at room temperature under a stream of dry N_2 at varying scan rates ranging from 20 to 500 mV s^{-1}. $N^nBu_4PF_6$ was used as a supporting electrolyte, being recrystallised from ethanol and oven dried prior to use, with a typical solution concentration of 0.2 M. The working electrode was a glassy carbon disc, Pt wire was the counter electrode. The reference electrode was Ag/AgCl, being chemically isolated from the analyte solution by an electrolyte containing bridge tube tipped with a porous frit. Ferrocene was employed as an internal reference, with all potentials quoted relative to the Fc/Fc^+ couple.

X-Ray crystallography. Diffraction data were recorded on a Bruker Smart CCD area detector with an Oxford Cryosytems low temperature system. The typical experimental T was 100 K, with an X-ray wavelength of 0.71073 Å. Reflections were measured from a hemisphere of data collection frames, each covering ω = 0.3°. All reflections were corrected for Lorentz and polarisation effects and for absorption by semi-empirical methods based on symmetry-equivalent and repeated reflections. The structure was solved by direct methods and refined by full-matrix least-squares on F^2.

Time-resolved infrared spectroscopy. These studies were conducted at the Rutherford Appleton Laboratory, laser for Science Facility, STFC, UK. The set-up and experimental procedures are described in detail elsewhere.[24]

Photoacoustic calorimetry, PAC. TiO_2 films were prepared by screen printing one layer of TiO_2 colloid paste (Ti-Nanoxide HT/SO, Solaronix) onto glass microscope slides and by gradually heating at 125 °C for 10 min, 325 °C for 5 min, 375 °C for 10 min, 450 °C for 10 min and 500 °C for 15 min. A film was dyed with MnTPPS (5,10,15,20-tetrakis(4-sulphonylphenyl)-porphyrinate manganese(III) acetate) for several hours to give an optical density of approximately 0.2 at the excitation wavelength. Separate films were dyed with **1a** and **2a** from DMF solutions, with optical density at 585 nm (**1a**) and 526 nm (**2a**) matching that of the $MnTPPS/TiO_2$ film. Pulsed laser excitation was achieved by the output of an EKSPLA PG122/SH OPO pumped by the third harmonic of an EKSPLA NL301G Nd:YAG laser at a frequency of 10 Hz. A small fraction of the laser beam was reflected to a photodiode and used to trigger the transient recorder oscilloscope (Tektronix DSA 601, 1 Gs s^{-1}). Photoacoustic waves were detected with a 2.25 MHz Panametrics transducer (model 5676). The photoacoustic wave obtained with the MnTPPS dye was used as photoacoustic reference.[36] Typically, 200 PAC waves from the samples (TiO_2 with dye **1a** or **2a**), reference (TiO_2 with MnTPPS) or background (TiO_2 only) immersed in acetonitrile were recorded and averaged under the same conditions. Four sets of averaged sample and background waves were used for data analysis at each laser intensity, with four laser intensities being used in each experiment by interposing neutral density filters with $\%T$ between 26% and 84% in the laser beam.

The PAC experiments measure the pressure wave generated upon conversion of excitation energy into heat, as the electronically excited dye evolves to a long lived charge separated state with the electron located in the conduction band of the semiconductor, and the formation of the dye cation. PAC experiments separate several processes which can contribute to heat deposition into the medium by their characteristic lifetimes. A 2.25 MHz transducer employed in the experiments described here allows one to investigate processes associated with the deposition of heat operating in three "time regimes":

1) For the processes occurring in the time frame shorter than 10 ns, an integrated amount of heat deposited is recorded;

2) For the processes occurring in the time range between ~10 ns and ~500 ns the kinetics of the heat deposition can be resolved;

3) For the processes occurring on a timescale longer than ~500 ns, no detection of heat deposition is possible.

Dye adsorption studies. Titanium dioxide paste (Ti-Nanoxide HT/SO, Solaronix) was deposited onto a glass slide through the screen printing technique with an area of 1 cm^2. The resulting films were gradually heated (up to 500 °C). Morphology and thickness of the TiO_2 films (1.2 μm) was analysed by electron microscopy (SEM).

TiO_2 films were immersed in the solutions of the dyes in DMF (50 μM), and UV-Vis absorption spectra taken at selected time intervals, from 20 s to 210 min. The amount of adsorbed dye was monitored as a function of time by measuring the absorbance of the dye-modified TiO_2 films at the wavelength of maximum absorption using a Shimadzu UV-2100 UV-Vis spectrophotometer. Excess dye was removed by rinsing with DMF followed by ether or ethanol before the absorption spectrum was registered. For the de-adsorption studies, the films were in contact with a few drops of NaOH (0.1 M) and then immersed in DMF (3 mL). The total amount of the dye adsorbed on the TiO_2 films was determined through the subsequent measurement of a UV-Vis absorption spectra and use of the solution-phase extinction coefficient.

Cell preparation and measurements. The titanium dioxide paste (Ti-Nanoxide HT/SO, Solaronix) was deposited onto transparent conducting glass (2.2 mm tick, 7 ohm per sq FTO, Solaronix) by the 'doctor-blade' technique, giving 1 cm^2 films with 5 μm thickness. Films were dried at 125 °C for 15 min and then a 2 μm thick layer of TiO_2 paste (Ti-Nanoxide D20/SP, Solaronix) was deposited using a screen-printing method. The double-layered films were gradually heated at 125 °C for 10 min, 325 °C for 5 min, 375 °C for 10 min, 450 °C for 10 min and 500 °C for 15 min.

After cooling, the TiO_2 electrode was further treated with a 40 mM $TiCl_4$ aqueous solution at 70 °C for 30 min and then calcined at 500 °C for 30 min. When the temperature was reduced to 80 °C, the TiO_2 electrode was immersed into a freshly prepared dye solution for a period of 12 h in the dark. The electrode was rinsed and dried. A thin Pt layer (Pt-Catalyst

T/SP Solaronix) was deposited onto transparent conducting glass by the 'doctor-blade' technique and used as the counter electrode. The two electrodes were sealed together using polymer film (25 μm, Solaronix) in a sandwich-type cell. Electrolyte was introduced through holes drilled in the counter electrode, subsequently sealed with microscope slides and polymer film to avoid leakage of the electrolyte solution.

The current–voltage (*J*–*V*) curve were measured by a Metrohm Autolab PGSTAT 10 electrochemical analyser using a 150 W Solar Simulator (100 mW cm^{-2}, AM 1.5 G) (Newport Oriel) for illumination. The electrolyte used for performance measurements consists of 0.6 M 1-butyl-3-methylimidazolium iodide, 0.03 M iodine, 0.10 M guanidinium thiocyanate, 0.50 M *tert*-butyl pyridine in a solution of acetonitrile–valeronitrile (85 : 15 (v/v)). The DSSCs were masked to expose only the active area (1 cm^2) under irradiation for all measurements.

Results and discussion

Synthesis

The ester-functionalised diimine Pt(II) catecholates **1** and **2** were prepared *via* a 'two-pot' method, whereby the appropriate catechol was first deprotonated with ^{t}BuOK in anhydrous THF prior to complexation with {(COO^{i}Pr)$_2$bpy}PtCl$_2$. It was noted that carrying out the complexation reaction in alcoholic solvents resulted in loss of the diisopropylacetate functionality through base mediated trans-esterification. For example, performing the reaction in MeOH produced {(COOMe)$_2$bpy}Pt(catechol), with trans-esterification being rapid and quantitative. The resultant Pt(II) catecholate products were readily purified by column chromatography, giving very dark blue coloured solids found to be soluble in the majority of common laboratory solvents. Conversion of **1** and **2** to the corresponding carboxylic acid-containing species (**1a** and **2a**) was effected through KOH mediated hydrolysis in a THF–H_2O solvent system.[40] The final 'dye' molecules **1a** and **2a** were found to be sparingly soluble in all solvents apart from DMF and DMSO (Fig. 1).

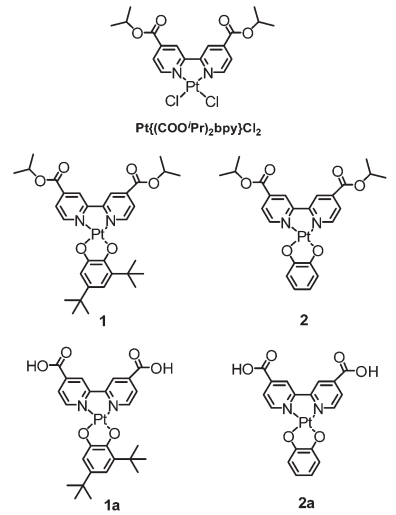

Fig. 1 Structures of the Pt(II) diimine complexes investigated in this study. **1**, **{(COO^{i}Pr)$_2$bpy}Pt(^{t}Bu$_2$Cat)** and **2** **{(COO^{i}Pr)$_2$bpy}Pt(pCat)** are the ester-functionalised parent complexes, the corresponding acid-containing **1a** and **2a** are investigated herein as sensitisers for DSSCs.

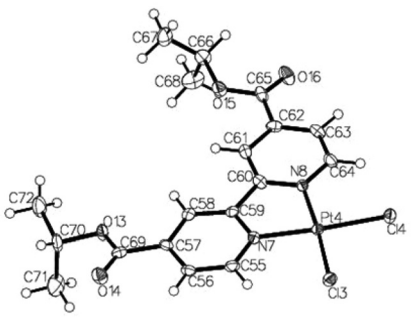

Fig. 2 X-ray crystal structure of {(COO^{i}Pr)$_2$bpy}PtCl$_2$. Brilliant orange coloured crystals suitable for X-ray diffraction 0.43 × 0.12 × 0.12 mm^3 were grown from the slow vapour diffusion of Et_2O into a CH_2Cl_2 solution of the dichloride complex. Selected bond lengths (Å) and angles (°): Pt(1)–N(1) 2.005(4), Pt(1)–N(2) 2.010(4), Pt(1)–Cl(5) 2.2947(13), Pt(1)–Cl(6) 2.2968(12), N(1)–Pt(1)–N(2) 80.76(16), Cl(5)–Pt(1)–Cl(6) 89.36(5), N(1)–Pt(1)–Cl(6) 94.77(12), N(2)–Pt(1)–Cl(5) 95.08(12). CCDC 1028955.

X-ray crystallography

Single crystals were grown for the dichloride precursor {(COO^{i}Pr)$_2$bpy}PtCl$_2$ and Pt(II) catecholate **2** (Fig. 2 and 3). The crystal structure of {(COO^{i}Pr)$_2$bpy}PtCl$_2$ reveals the Pt(II) centre to be in a distorted square planar coordination environment, with the bond angle between the two chelating nitrogen atoms and the metal centre N(1)–Pt–N(2) being 80.76°. The 4,4′-substituted-2,2′-bipyridine ligand is close to being planar, with a dihedral angle between the two pyridyl rings of 3.45°. This value is consistent with that measured previously for similar diimine Pt(II) complexes.[17] The crystal structure of **2** (Fig. 3) also shows the expected distorted square planar geometry as a result of the two bidentate ligands, with N(1)–Pt–N(2) and O(1)–Pt–O(2) being 80.97° and 84.22° respectively. The torsion angle between the two aforementioned planes is determined to be 2.17°, revealing the complex to be essentially planar. Both **2** and {(COO^{i}Pr)$_2$bpy}PtCl$_2$ stack in dimer-like 'head-to-tail' pairs, facilitated by short Pt···Pt contacts,[41] with the intermetal distances measured to be 3.56 Å and 3.52 Å respectively. In the former instance, these metal–metal interactions appear to be supported by additional π–π interactions between the bipyridyl and pyrocatechol ligands within each pair.

Electronic absorption spectroscopy

UV-Vis-NIR electronic absorption spectra for DMF solutions of complexes **1**, **1a**, **2**, **2a** and the dichloride precursor {(COO^{i}Pr)$_2$bpy}PtCl$_2$ are shown in Fig. 4. All complexes show an intense absorption band in the region of 300 nm, assigned to π–π* intra-ligand transitions localised upon the bipyridine moiety. The spectrum recorded for {(COO^{i}Pr)$_2$bpy}PtCl$_2$ reveals an additional, less intense band centered at 415 nm. This tran-

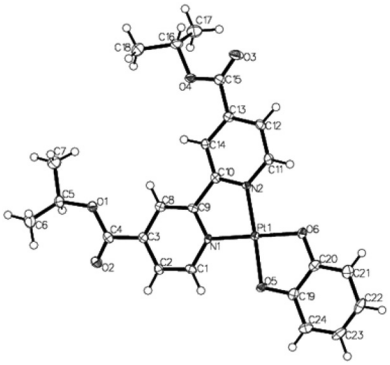

Fig. 3 X-ray crystal structure of **2**. Deep blue coloured crystals were grown from the slow evaporation of a mixed toluene–CH_2Cl_2 solution at room temperature. Selected bond lengths (Å) and angles (°): Pt(1)–N(1) 1.983(3), Pt(1)–N(2) 1.994(3), Pt(1)–O(5) 1.986(2), Pt(1)–O(6) 2.005(2), N(1)–Pt(1)–N(2) 95.68(11), O(5)–Pt(1)–O(6) 84.22(10), N(1)–Pt(1)–O(5) 95.68(11), N(2)–Pt(1)–O(6) 99.16(11). CCDC 1028956.

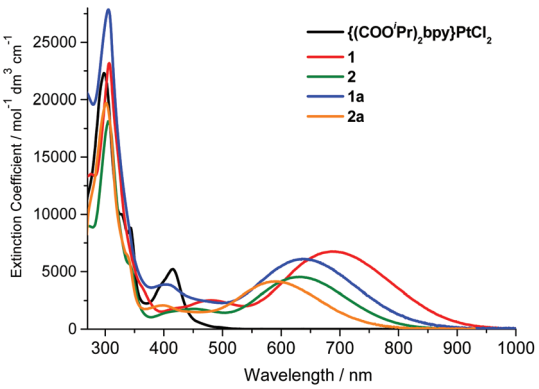

Fig. 4 Ground state electronic absorption spectra for DMF solutions of Pt(II) catecholates **1**, **2**, **1a**, **2a** and the dichloride precursor {(COO^{i}Pr)$_2$bpy}PtCl$_2$, recorded at room temperature.

sition is attributed to a metal-to-ligand charge transfer (MLCT), a feature observed in (diimine)$PtCl_2$ type complexes reported previously, where the transition has been more stringently described as a 'charge transfer-to-diimine' owing to the chloride ligands making an appreciable contribution to the HOMO.[42] The absorption spectra of the catecholates are dominated by a broad, low-energy band which extends into the NIR region. This band is characteristic of Pt(II) catecholates, with its' absence in the spectrum of {(COO^{i}Pr)$_2$bpy}$PtCl_2$ allowing primary assignment to a ligand-to-ligand charge transfer (LL'CT).[16,17,20,43] However, since the electronic transition between catechol and diimine ligands is known to also involve orbital contributions from the metal centre, the process may be more accurately labelled as a mixed metal–ligand-to-ligand charge transfer (MMLL'CT).[21] It is noted that the change in catechol ligand between **1** and **2** is manifest in the electronic absorption spectra. The inclusion of tertiary butyl substituents in **1** is seen to shift the maximum of the low energy CT band by approximately 60 nm below that observed for **2**. This is attributed to the weakly electron-donating alkyl groups destabilising the catechol based HOMO, thus reducing the HOMO–LUMO energy gap and the energy of the corresponding transition. It is also observed that hydrolysis of the ester groups results in a shift of the MMLL'CT band to a higher energy in both instances, being approximately 1300 cm^{-1} and 1200 cm^{-1} above that observed for the parent esters of **1a** and **2a** respectively.

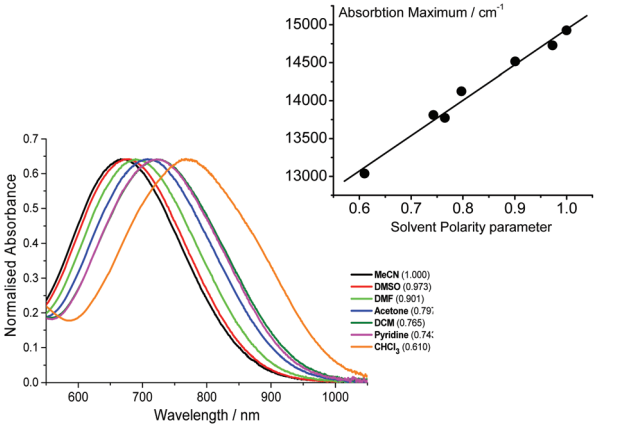

Fig. 5 Ground state electronic absorption spectra of **1** recorded in a variety of solvents, exemplifying the negative solvatochromic behaviour of the lowest energy absorption band. The solvent polarity parameters[46] are shown within brackets. The inset shows the linear correlation between the energy of the CT state and solvent polarity, with a slope (solvatochromic shift) of 4665 cm^{-1} (0.578 eV).

Solvatochromism of the absorption spectra

The CT nature of the lowest energy absorption band is further verified through solvatochromism. Previously, CT transitions in Pt(II) catecholates have been shown to display negative solvatochromism; namely, the shift of the MMLL'CT band maximum to lower energy with decreasing solvent polarity.[16,20] This behaviour is clearly exemplified for **1** in Fig. 5, where electronic absorption spectra recorded in a range of solvents are displayed. The red-shift of absorption maxima from 673 nm in MeCN to 768 nm in $CHCl_3$ is indicative of an inversion, or decrease in magnitude, of the dipole moment upon formation of the catechol-to-diimine CT state.[44,45] The inset within Fig. 5 illustrates the linear correlation between absorption energy and solvent polarity parameter derived for Pt(II) dimine complexes,[46] with a solvatochromic shift (slope) of 4665 cm^{-1} (0.578 eV), consistent with a CT-type transition.

Electrochemistry

Cyclic voltammograms were recorded for CH_2Cl_2 solutions of **1**, **2** and the dichloride precursor {(COO^{i}Pr)$_2$bpy}$PtCl_2$ across the potential range +1.2 to −2.2 V *vs.* Fc/Fc^+ (Fig. 6).

Reduction. All complexes investigated by cyclic voltammetry were found to display two reduction processes within the potential window shown below in Fig. 6. Based on the ΔE values (Table 1), for the dichloride precursor, {(COO^{i}Pr)$_2$bpy}-$PtCl_2$, both reductions can be considered fully electrochemically reversible, whereas for the Pt(II) catecholates only the first

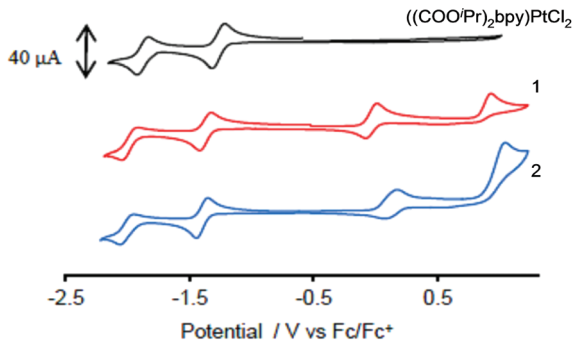

Fig. 6 Cyclic voltammograms for 1.8 mM CH_2Cl_2 solutions of {(COO^{i}Pr)$_2$bpy}PtCl$_2$ (top), **1** (middle) and **2** (bottom). Scans shown were recorded at 100 mV s^{-1} at room temperature with 0.2 M NBu_4PF_6 as supporting electrolyte. All potentials are quoted against Fc/Fc$^+$.

Table 1 Electrochemical data for r. t. 1.8 mM CH_2Cl_2 solutions of **1**, **2**, and related compounds, potentials are quoted *vs.* the Fc/Fc$^+$ couple (+0.43 V *vs.* sce under conditions used). Anodic–cathodic peak separation, mV, given in brackets where appropriate ($\Delta E_{a,c}$ for Fc/Fc$^+$ is typically 90 mV). τ, excited state lifetimes, obtained by TRIR in CH_2Cl_2 at r.t., also included

	Reduction/V	Oxidation/V	τ, ps
{(COO^{i}Pr)$_2$bpy}PtCl$_2$	−1.26 (99)		
	−1.87 (91)		
1	−1.37 (92)	−0.03 (95)	
	−1.98 (131)[a]	+0.93[b]	250
2	−1.39 (95)	+0.11 (124)[a]	
	−2.00 (113)[a]	+1.05[b]	
Pt(bpyam)(^{t}Bu$_2$cat)	−1.59[c]		420
Pt(^{t}Bubpy)(^{t}Bu$_2$cat)	−1.81[c]		630

[a] Electrochemically quasi-reversible process. [b] Chemically irreversible under the experimental conditions. [c] From ref. 16.

reduction is electrochemically reversible with the second being electrochemically quasi-reversible.

The occurrence of these electrochemical features in all complexes allow the processes to be assigned to the sequential reduction of the bipyridine fragment. The influence of the weakly electron-withdrawing ester functionality may be quantified through comparison with similar Pt(II) catecholates where an unsubstituted 2,2′-bipyridine analogue of **1** gives a first reduction potential at −1.74 V and a 4,4′-di-*tert*-butyl-2,2′-bipyridine version a more cathodic reduction at −1.82 V.[47] It is concluded that for the complexes studied here, both the LUMO and LUMO+1 are localised mainly upon the bipyridine moiety.

Oxidation. Two oxidation processes were observed for both **1** and **2**, the absence of which in {(COO^{i}Pr)$_2$bpy}PtCl$_2$ indicates that these processes are associated with the coordinated catechol fragments. The first oxidation was found to be electrochemically reversible for **1** and quasi-reversible for **2**, with the second process being chemically irreversible in both instances. Indeed, two such electrochemical oxidations have been readily observed for Pt(II) catecholates previously, with it being well established that the former relates to a catechol-to-semiquinone conversion and the latter to further oxidation of the fragment to a quinone form.[17,19,21] The influence of the two weakly electron-donating tertiary butyl groups in **1** is manifested through the occurrence of the first oxidation at a marginally more cathodic potential than that observed for **2**. It is concluded that both the HOMO and HOMO−1 for **1** and **2** reside on the catechol fragment.

Picosecond time-resolved infrared spectroscopy

The lifetime of the excited state of **1** in fluid solution was obtained by TRIR spectroscopy, in the detection range from 1400 to 1800 cm^{-1}. Excitation of a solution of **1** in CH_2Cl_2 with 400 nm, ~50 fs laser pulse lead to instantaneous bleaching of the ground state IR absorption bands, and the formation of transient signals across the fingerprint region (Fig. 7).

The early time dynamics (before 5 ps) are difficult to resolve due to very broad signals around 1600 cm^{-1}, which for similar complexes were previously assigned to vibrationally hot water molecules associated with the catechol moiety.[24] After *ca.* 5 ps, the spectral dynamics can be satisfactorily described with the 250 (±50) ps lifetime, using global fit analysis. The corresponding kinetic traces and fitting curves are shown in Fig. 7. The observed spectral features are very similar to those observed by us previously for other Pt(diimine)(catecholate)

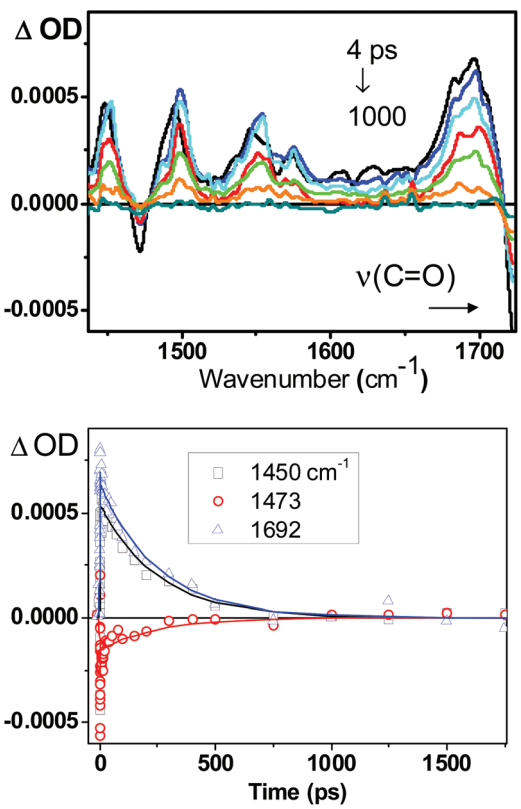

Fig. 7 Picosecond time-resolved infrared spectroscopic data of 1 mM solution of **1** in CH_2Cl_2 at r.t. following 400 nm, ~50 fs excitation. Top: spectra at selected delay times after the excitation pulse; bottom: kinetic traces at selected frequencies (symbols) and the global fit to the data (solid lines).

compounds[16,24] and are consistent with the ML/LLCT assignment of the excited state detected. The 250 ps value of the lifetime of the charge-transfer state in **1** forms a trend with the 420 ps and 630 ps lifetimes for the excited states of Pt(4,4′-(C(O)NEt$_2$)$_2$bpy)(^{t}Bu$_2$Cat), and Pt(4,4′-^{t}Bu$_2$bpy)(^{t}Bu$_2$Cat), resp.[16] In this series of compounds, which share the same donor ligand, ^{t}Bu$_2$Cat, the lifetime systematically increases with a decrease in electron-accepting ability of the diimine ligand, in accordance with the energy gap law.

Dye adsorption on TiO_2

Thin films (1.2 μm) of nanocrystalline TiO_2 deposited on glass slides were immersed in DMF solutions of dyes **1a** and **2a**. The resulting intense blue-purple colouration imparted on the TiO_2 films affirmed successful dye anchorage, with the corresponding UV-Visible absorption spectra of the surface adsorbed dyes being shown in Fig. 8. The spectra of the surface anchored dyes clearly show a broad band in the region of 575–650 nm and 500–575 nm for **1a** and **2a** respectively. These absorbance features correspond to the MMLL'CT bands observed in the solution phase spectra, although being notably broadened and blue-shifted in both instances. These spectra highlight one of the most favourable attributes of Pt(II) catecholates – their ability to harvest photons from across a large low-energy part of the visible region.

Dye loadings were investigated by monitoring the progress of dye adsorption: UV-Vis absorption spectra of the sensitised TiO_2 films were collected as a function of immersion time, with the surface being rinsed with DMF and Et_2O prior to each measurement to remove the non-adsorbed dye. Typical dye solution concentrations of 50 μM were employed so as to minimise dye agglomeration and reduce surface aggregation. The dye uptake plots for **1a** and **2a** are shown in Fig. 9. Both curves reveal the very rapid initial uptake of the dyes, with approximately 50% of the maximum observed surface coverage being achieved within the first 25 min immersion time. After this period the rate of dye uptake decreases in both instances. Monolayer surface coverage is determined to be

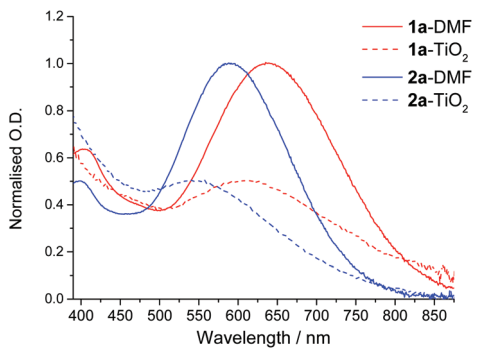

Fig. 8 UV-Visible electronic absorption spectra of **1a** and **2a** in DMF solutions (solid line), and when anchored onto thin film of TiO_2 (dashed line). Optical densities have been normalised at the absorbance maximum of the lowest energy band: solution OD = 1.0, adsorbed dye OD = 0.5.

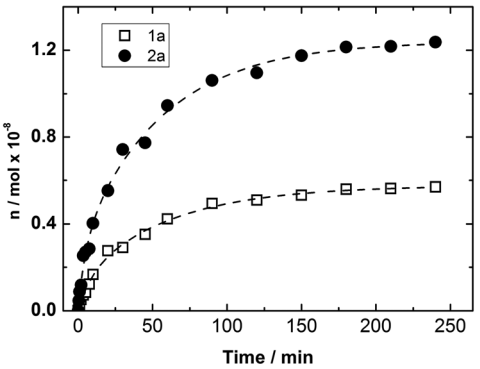

Fig. 9 Dye uptake curves for **1a** and **2a** onto TiO_2 film of thickness 1.2 μm from DMF solutions (50 μM) at room temperature. The curves are plotted as a function of immersion time. Maximum dye loading at monolayer surface coverage is determined to be approximately 0.5 × 10^{-8} and 1.2 × 10^{-8} mol cm^{-2} for **1a** and **2a** respectively.

reached when the rate of change of surface adsorbed dye concentration reaches zero, being observed here after approximately 175 min immersion time for both dyes. Desorption of the dyes with NaOH and use of the solution phase extinction coefficient allows monolayer surface loading to be defined as 0.5 × 10^{-8} and 1.2 × 10^{-8} mol cm^{-2} for **1a** and **2a** respectively. Allowing for a consideration of the thickness (1.2 μm) of the films used within this study, the magnitude of this loading is comparable with that which has been reported for Pt(II) thiolate dyes,[28,29] although with longer immersion times being required due to the lower dye solution concentrations utilised here.[48]

With the mode and position of surface attachment being identical for both dyes, the higher loading achieved with **2a** is attributed directly to the planar nature of this Pt(II) catecholate. Favourable π–π stacking interactions between the pyrocatechol entities, together with short Pt···Pt contacts, are likely to facilitate the close packing of the dye when adsorbed on a semi-conductor surface. The inclusion of tertiary butyl substituents in **1a** affords the dye with a significantly greater steric bulk, thus hindering close surface packing and reducing the maximum possible monolayer surface loading by a factor of approx. 2.5.

Photoacoustic calorimetry (PAC)

MnTPPS adsorbed onto a TiO_2 film was employed as a photoacoustic reference, and is defined as a dye which converts all absorbed energy into heat on a time-scale much shorter than that of the time-resolution of acoustic detection.[36] After subtraction of an almost negligible background signal, sample and reference PAC signals were compared, with no mis-match in phase, indicating that the release of heat from the sample also occurs on a time-scale faster than the acoustic detection time-resolution. Table 2 shows the values of photoacoustic wave maxima obtained from PAC performed on **1a** and **2a** anchored to thin film TiO_2, where ϕ denotes the fraction of heat released by the sample under study relative to the photo-

Table 2 Photoacoustic experimental data (observed wave maxima) for thin film TiO_2 sensitised with dyes **1a** and **2a** immersed in acetonitrile. The wavelengths of excitation were 585 nm (2.12 eV) and 526 nm (2.36 eV) for **1a** and **2a**, respectively. The laser energy at 100% power was 50 μJ per pulse. The tabulated data are averaged values of results collected in four independent experiments. The values of ϕ_{CS} were calculated using eqn (1) and (2), where $E(D/D^+)$ was the $E^{1/2}{}_{ox}$ *vs.* S.C.E., estimated error is 10%

	Dye **1a**				Dye **2a**			
Relative laser intensity/%	Reference/mV	Sample/mV	ϕ	ϕ_{cs}	Reference/mV	Sample/mV	ϕ	ϕ_{cs}
100	71	58	0.92		69	63	0.81	
84	63	48	0.92		61	56	0.77	
52	48	37	0.86		46	40	0.78	
26	35	28	0.93		33	31	0.79	
		Average ϕ: 0.91		0.26		*Average ϕ: 0.79*		0.56

acoustic reference. The maxima of the photoacoustic waves were observed to be independent of the excitation laser pulse energy, indicating that no bi-photonic processes were occurring under the laser fluences used. From the experimentally obtained ϕ values, the quantum yield of formation of the long-lived charge separation (ϕ_{CS}) between the electron injected in the semiconductor and the oxidised dye can be calculated through eqn (1), where $E_{h\nu}$ is the energy of excitation and E_{cs} is the energy of the charge separated state. E_{cs} itself may be determined from eqn (2). We assume a negligible change in the first (catechol-based) oxidation potential upon hydrolysis of the ester functionality, therefore the measured potentials for the parent ester compounds **1** and **2** (Table 1) are used in eqn (2) and the following analysis.

$$\phi_{CS} = \frac{(1-\phi)E_{h\nu}}{E_{cs}} \quad (1)$$

$$E_{cs} = E(D/D^+) - E_{cb} \quad (2)$$

The PAC results for (1) and (2) showed signals only for the fast (<10 ns) heat deposition, which were assigned to charge injection and also account for the fast recombination of the injected electron with the oxidized sensitizer that occurs on a time scale less than 10 ns. No signal on the longer timescale was detected, therefore the energy not released as heat is assigned to the formation of the long-lived, >500 ns, charge separated state between the sensitizer S^+ and the semiconductor ($TiO_2^{\bullet-}$). We stress that this way of estimating the yield of electron injection, through the yield of long-lived charge-separation, does not reflect the instantaneous injection only, but also takes into account the recombination processes on the fast, <10 ns, timescale. Thus the value quoted here is the yield of electron transfer to the semiconductor from the photo-excited sensitizer, which remains after 10 ns time.

Here, we consider that dye sensitised TiO_2 electrodes exhibit an exponential density of states extending into the TiO_2 band gap. Since a low excitation light intensity leads to a low density of photoinjected electrons, the majority of these electrons will occupy states with energies close to the quasi-Fermi level.[49] Under such condition, the calculation of E_{cs} through eqn (2) with a single value is acceptable. Thus, using a value of −0.34 V (*vs.* SCE) for the energy of the TiO_2 conduction band (E_{cb})[50] we obtained values of 0.26 and 0.56 for the yields of long-lived dye-TiO_2 charge separation for **1a** and **2a**, respectively. A control experiment on the dye N719 (*cis*-bis(isothiocyanato)-bis(2,2′-bipyridyl-4,4′-dicarboxylato)-ruthenium(II)) performed under identical experimental conditions[37] yielded a 100% quantum yield of the formation of the charge separated state (assuming E_{cs} of 1.05 eV[37,51] for this dye), which is consistent with the previous results.[52]

It has been reported that the energy of the conduction band (E_{cb}) for thin film anatase TiO_2 depends upon the nature and composition of a contiguous electrolyte solution,[53] namely upon the presence of cations in the non-aqueous electrolytes,[54] in addition to the chemical nature of the sensitiser itself.[55] In this work, PAC studies were performed in neat acetonitrile, and it is therefore possible that the effective position of the conduction band may differ from the value considered above. Values as negative as −2 V (*vs.* SCE) have been reported for TiO_2 in contact with acetonitrile.[53] As a result, the values for the yield of formation of charge separated states estimated using PAC technique should be considered an upper limit.

The observed low dye-to-semi-conductor electron injection yields in sensitised TiO_2 films (in contact with MeCN) may be accounted for by a short excited state lifetime of the dyes. Results presented previously[56] have illustrated that a complete sensitised solar cell (including electrolyte) exhibits an approx. 20-fold retardation in the rate of electron injection in comparison to a dye-sensitised TiO_2 film. The addition of a redox electrolyte is, therefore, likely to reduce the electron injection efficiency further,[57] and therefore the quantum yields of electron injection determined through PAC (Table 2) may be substantially reduced upon incorporation of the dye into a complete functioning DSSC.

Photocurrent–voltage characteristics of Pt-Dye/TiO_2 electrodes

Photovoltaic device performance parameters were obtained for cells sensitised with dyes **1a** and **2a** (Table 3) with accompanying current–voltage curves generated under illumination with AM 1.5 G (100 mW cm^{-2}) simulated sunlight displayed in Fig. 10. It is apparent that cells sensitised with these particular Pt(II) complexes operate with a poor overall efficiency (η), being somewhat lower than other devices sensitised with Pt(II)

Table 3 Photovoltaic device performance parameters for cells sensitised with **1a** and **2a** (24 h immersion time). Measurements were taken under AM 1.5 G (100 mW cm^{-2}) simulated solar light, with a square-shaped mask of area 1 cm^2 being used in all experiments

Dye	J_{sc}/mA cm^{-2}	V_{oc}/V	FF	η/%
1a	0.14	0.37	0.47	0.02
2a	0.31	0.38	0.55	0.07

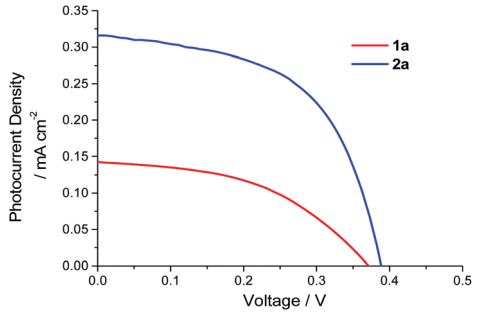

Fig. 10 Current–voltage curves for solar cells sensitised with dyes **1a** and **2a**. Measurements were taken under illumination with AM 1.5 G simulated solar radiation, mask area 1 cm^2.

diimine-based dyes ($\eta \approx 0.1$–3%)[28,30] and significantly below that achievable with the archetypal N719 dye.[58] Photovoltaic characteristics for cells sensitised with N719 under identical experimental conditions to those employed for **1a** and **2a** yield an overall device efficiency of 6% (J_{sc} = 14.6 mA cm^{-2}; V_{oc} = 0.67 V; FF = 0.61). These values are typical for cells employing high-efficiency dyes[48] and are used for comparison with the Pt(II) dyes investigated here. The low efficiency of Pt(II) catecholates as sensitisers may be explained by the short excited state lifetime. Both ourselves[16] and others[59] have shown the lifetime of the charge separated state in Pt(II)(diimine)(catechol) complexes, where an electron resides on the bipyridine fragment, to be on the picosecond time scale; the value of 250 ps obtained for 1 using TRIR is consistent with the previous observations for related complexes. As electron injection occurs from this excited state, the relatively short lifetime and rapid intramolecular charge recombination are expected to out-compete charge injection. Additionally, the low first oxidation potential associated with these Pt(II) catecholates is likely to hinder the efficient regeneration of the oxidised dye through electron transfer from the redox electrolyte, with recombination of injected electrons with the oxidised dye occurring more rapidly.[28] These features are akin to those reported for other Pt(II)-centred sensitisers, particularly those which absorb photons from across the low-energy portion of the solar spectrum.[29] The performance of **1a** and **2a** with respect to N719 could also be decreased by a lower absorption of light: it is estimated that 5 μm thick TiO_2 films dyed with N719 absorb in excess of 90% of incident light at the wavelength of maximum absorption, compared with around 60% for the films containing either **1a** or **2a**.

Devices containing **2a** yield a higher photocurrent density and greater overall device efficiency than those employing **1a** (Table 3). Since the chemical and photophysical properties of the two Pt(II) catecholates are very similar, and the optical densities used are also comparable, the difference in device performance may be attributed directly to the degree of surface loading.

The magnitude of the improvement in efficiency upon moving from **1a** to **2a** is consistent with the 2.5-fold increase in monolayer surface coverage achievable in the latter instance. This conclusion is consistent with the data obtained by PAC, where the yield of formation of charge separation was found to be approximately 2.5 times greater for **2a** than **1a** anchored on a semiconductor.

Conclusion

Pt(II) diimine catecholates which intensely absorb in the red part of the visible spectrum are potentially promising candidates for light-driven applications. Here, we test their potential as sensitisers in dye-sensitised solar cells, and correlate this property with the efficiency of charge separation, evaluated by photoacoustic calorimetry (PAC). Two 2,2′-bipyridine-4,4′-di-carboxylic acid-containing Pt(II) catecholates have been prepared from their parent iso-propyl ester derivatives, and their photophysical and electrochemical properties studied. Solution phase electronic absorption spectra show intense charge transfer bands which extend into the NIR region, the energy of which may be readily tuned through substituent variation upon the diimine and catechol ligands. Modifying diimine Pt(II) catecholates with carboxylic acid functionality has allowed for the successful anchoring of these complexes to thin film TiO_2, where steric bulk of the donor ligands (*t*Bu-catechol *vs.* catechol) has been found to significantly influence the extent of monolayer surface coverage. In this instance, **2a** bearing an unsubstituted cathecol shows a 2.5-fold increase in surface loading over **1a**, which contains a bulkier *t*Bu-catecholate ligand. Photovoltaic measurements on solar cells sensitised with **1a** and **2a** have allowed for an assessment as to the suitability of these complexes as sensitisers. The observed 0.02–0.07% device efficiency is attributed to the short excited state lifetime and rapid charge recombination dynamics inherent to this class of complex. Specifically, the lifetime of the charge-transfer ML/LLCT excited sate in the parent complex **1** was determined as 250 ps by time-resolved infrared spectroscopy, TRIR. The measured increase in device efficiency for **2a** over **1a** is consistent with a similar increase in the quantum yield of the long-lived charge separated state (where the complex acts as a donor and the semiconductor as an acceptor) as determined by Photo-Acoustic Calorimetry, and is also matching the magnitude of the increased surface loading achieved with **2a**. It is concluded that the relative efficiency of devices sensitised with these particular Pt(II) species is governed by the degree of surface coverage. Overall, this work demonstrates for the first time the use of

Pt(diimine)(catecholate) complexes as potential photo-sensitizers in solar cells: the intense absorption in the visible/NIR part of the spectrum is a strong advantage of these dyes, whilst the short excited state lifetime can in the future be addressed by modifying the diimine ligands involved.

Acknowledgements

We thank the EPSRC, E-Futures DTC, the STFC, the University of Sheffield, and the Coimbra Chemistry Centre from the FCT (project PEst-OE/QUI/UI0313/2014) for financial support. We are also grateful for the receipt of a Santander research mobility award (JAW and PAS), and to Johnson Matthey for the generous loan of Pt(II) salts. We thank Prof. M. Towrie and Prof. M. Ward for fruitful collaboration. The research leading to the results presented herein has received funding from the European Community's FP7 under grant agreement number 228334 (Laser Lab Europe II). PJ and CS acknowledge support for project PTDC/QUI/QUI/099730/2008 from Fundação para a Ciência e a Tecnologia (Portugal) through the COMPETE programme and from FEDER (European Union).

References

1 M. Haga, E. S. Dodsworth and A. B. P. Lever, *Inorg. Chem.*, 1986, **25**, 447–453.
2 S. Bhattacharya and C. G. Pierpont, *Inorg. Chem.*, 1994, **33**, 6038–6042.
3 M. R. Churchill, K. M. Keil, B. P. Gilmartin, J. J. Schuster, J. B. Keister and T. S. Janik, *Inorg. Chem.*, 2001, **40**, 4361–4367.
4 S. Bhattacharya, S. R. Boone, G. A. Fox and C. G. Pierpont, *J. Am. Chem. Soc.*, 1990, **112**, 1088–1096.
5 A. M. Barthram, R. L. Cleary, J. C. Jeffery, S. M. Couchman and M. D. Ward, *Inorg. Chim. Acta*, 1998, **267**, 1–5.
6 P. R. Auburn, E. S. Dodsworth, M. Haga, W. Liu, W. A. Nevin and A. B. P. Lever, *Inorg. Chem.*, 1991, **30**, 3502–3512.
7 S. Patra, B. Sarkar, S. M. Mobin, W. Kaim and G. K. Lahiri, *Inorg. Chem.*, 2003, **42**, 6469–6473.
8 A. P. Meacham, K. L. Druce, Z. R. Bell, M. D. Ward, J. B. Keister and A. B. P. Lever, *Inorg. Chem.*, 2003, **42**, 7887–7896.
9 A. M. Barthram, Z. R. Reeves, J. C. Jeffery and M. D. Ward, *J. Chem. Soc., Dalton Trans.*, 2000, 3162–3169.
10 M. Haga, K. Isobe, S. R. Boone and C. G. Pierpont, *Inorg. Chem.*, 1990, **29**, 3795–3799.
11 F. Hartl and A. Vlcek, *Inorg. Chem.*, 1996, **35**, 1257–1265.
12 G. A. Abakumov, V. K. Cherkasov, K. G. Shalnova, I. A. Teplova and G. A. Razuvaev, *J. Organomet. Chem.*, 1982, **236**, 333–341.
13 K. A. M. Creber and J. K. S. Wan, *J. Am. Chem. Soc.*, 1981, **103**, 2102–2104.
14 M. D. Ward and J. A. McCleverty, *J. Chem. Soc., Dalton Trans.*, 2002, 275–288.
15 W. P. Griffith, *Transition Met. Chem.*, 1993, **18**, 250–256.
16 J. Best, I. V. Sazanovich, H. Adams, R. D. Bennett, E. S. Davies, A. J. H. M. Meijer, M. Towrie, S. A. Tikhomirov, O. V. Bouganov, M. D. Ward and J. A. Weinstein, *Inorg. Chem.*, 2010, **49**, 10041–10056.
17 N. M. Shavaleev, E. S. Davies, H. Adams, J. Best and J. A. Weinstein, *Inorg. Chem.*, 2008, **47**, 1532–1547.
18 B. Hirani, J. Li, P. I. Djurovich, M. Yousufuddin, J. Oxgaard, P. Persson, S. R. Wilson, R. Bau, W. A. Goddard and M. E. Thompson, *Inorg. Chem.*, 2007, **46**, 3865–3875.
19 W. Paw and R. Eisenberg, *Inorg. Chem.*, 1997, **36**, 2287–2293.
20 S. S. Kamath, V. Uma and T. S. Srivastava, *Inorg. Chim. Acta*, 1989, **166**, 91–98.
21 J. A. Weinstein, M. T. Tierney, E. S. Davies, K. Base, A. A. Robeiro and M. W. Grinstaff, *Inorg. Chem.*, 2006, **45**, 4544–4555.
22 V. Anbalagan and T. S. Srivastava, *Polyhedron*, 2004, **23**, 3173–3183.
23 P. L. Hill, L. Y. Lee, T. R. Younkin, S. D. Orth and L. McElwee-White, *Inorg. Chem.*, 1997, **36**, 5655–5657.
24 N. Deibel, D. Schweinfurth, S. Hohloch, M. Delor, I. V. Sazanovich, M. Towrie, J. A. Weinstein and B. Sarkar, *Inorg. Chem.*, 2014, **53**, 1021–1031.
25 N. Deibel, D. Schweinfurth, J. Fiedler, S. Zalis and B. Sarkar, *Dalton Trans.*, 2011, **40**, 9925–9934.
26 M. Gratzel, *J. Photochem. Photobiol., C*, 2003, **4**, 145–153.
27 M. Gratzel, *Inorg. Chem.*, 2005, **44**, 6841–6851.
28 A. Islam, H. Sugihara, K. Hara, L. P. Singh, R. Katoh, M. Yanagida, Y. Takahashi, S. Murata, H. Arakawa and G. Fujihashi, *Inorg. Chem.*, 2001, **40**, 5371–5380.
29 E. A. M. Geary, N. Hirata, J. Clifford, J. R. Durrant, S. Parsons, A. Dawson, J. Yellowlees and N. Robertson, *Dalton Trans.*, 2003, 3757–3762.
30 E. A. M. Geary, L. J. Yellowlees, L. A. Jack, I. D. H. Oswald, S. Parsons, N. Hirata, J. R. Durrant and N. Robertson, *Inorg. Chem.*, 2005, **44**, 242–250.
31 E. C.-H. Kwok, M.-Y. Chan, K. M.-C. Wong, W. H. Lam and V. W.-W. Yam, *Chem. – Eur. J.*, 2010, **16**, 12244–12254.
32 L. G. Arnaut, M. Barroso and C. Serpa, *Applied Photochemistry*, ed. R. Evans, H. D. Burrows and P. Douglas, Springer-Verlag, Dordrecht, 2013, pp. 267–304.
33 R. Katoh, A. Furube, T. Yoshihara, K. Hara, G. Fujihashi, S. Takano, S. Murata, H. Arakawa and M. Tachiya, *J. Phys. Chem. B*, 2004, **108**, 4818–4822.
34 R. Eichberger and F. Willig, *Chem. Phys.*, 1990, **141**, 159–173.
35 S. E. Koops, B. C. O'Regan, P. R. F. Barnes and J. R. Durrant, *J. Am. Chem. Soc.*, 2009, **131**, 4808–4818.
36 C. Serpa, J. Schabauer, A. P. Piedada, C. J. P. Monteiro, M. M. Pereira, P. Douglas, H. D. Burrows and L. G. Arnaut, *J. Am. Chem. Soc.*, 2008, **130**, 8876–8877.
37 P. J. Holliman, M. Mohsen, A. Connell, M. L. Davies, K. Al-Salihi, M. B. Pitak, G. J. Tizzard, S. J. Coles,

R. W. Harrington, W. Clegg, C. Serpa, O. H. Fontes, C. Charbonneau and M. J. Carnie, *J. Mater. Chem.*, 2012, **22**, 13318–13327.
38 T. Gensch and C. Viappiani, *Photochem. Photobiol. Sci.*, 2003, **2**, 699–721.
39 J. H. Price, A. N. Williamson, R. F. Schramm and B. B. Wayland, *Inorg. Chem.*, 1972, **11**, 1280–1284.
40 P. Jarosz, P. Du, J. Schneider, S.-H. Lee, D. McCamant and R. Eisenberg, *Inorg. Chem.*, 2009, **48**, 9653–9663.
41 J. J. Novoa, G. Aullon, P. Alemany and S. Alvarez, *J. Am. Chem. Soc.*, 1995, **117**, 7169–7171.
42 I. V. Sazanovich, M. A. H. Alamiry, J. Best, R. D. Bennett, O. V. Bouganov, E. S. Davies, V. P. Grivin, A. J. H. M. Meijer, V. F. Plyusnin, K. L. Ronayne, A. H. Shelton, S. A. Tikhomirov, M. Towrie and J. A. Weinstein, *Inorg. Chem.*, 2008, **47**, 10432–10445.
43 S. Shukla, S. S. Kamath and T. S. Srivastava, *J. Photochem. Photobiol., A*, 1989, **47**, 287–298.
44 T. R. Miller and I. G. Dance, *J. Am. Chem. Soc.*, 1973, **95**, 6970–6979.
45 D. M. Manuta and A. J. Lees, *Inorg. Chem.*, 1986, **25**, 3212–3218.
46 S. D. Cummings and R. Eisenberg, *J. Am. Chem. Soc.*, 1996, **118**, 1949–1960.
47 J. Best, PhD thesis, University of Sheffield, 2009.
48 C.-R. Lee, H.-S. Kim, I.-H. Jang, J.-H. Im and N.-G. Park, *ACS Appl. Mater. Interfaces*, 2011, **3**, 1953–1957.
49 J. N. Clifford, E. Palomares, M. K. Nazeeruddin, M. Gratzel, J. Nelson, X. Li, N. L. Long and J. R. Durrant, *J. Am. Chem. Soc.*, 2004, **126**, 5225–5233.
50 S. K. Haram, *Handbook of Electrochemistry*, ed. C. G. Zoski, Elsevier, Amsterdam, 1st edn, 2007.
51 M. K. Nazeeruddin, S. M. Zakeeruddin, R. Humphry-Baker, M. Jirousek, P. Liska, N. Vlachopoulos, V. Shklover, C. H. Fischer and M. Gratzel, *Inorg. Chem.*, 1999, **38**, 6298–6305.
52 R. Katoh, A. Huijser, K. Hara, T. J. Savenije and L. D. A. Siebbeles, *J. Phys. Chem. C*, 2007, **111**, 10741–10746.
53 J. E. Moser, *Dye Sensitised Solar Cells*, ed. K. Kalyanasundaram, EPFL Press, Lausanne, 1st edn, 2010.
54 H. Wang and L. M. Peter, *J. Phys. Chem. C*, 2012, **116**, 10468–10475.
55 T. Moehl, H. N. Tsao, K.-L. Wu, H.-C. Hsu, Y. Chi, E. Ronca, F. D. Angelis, M. K. Nazeeruddin and M. Gratzel, *Chem. Mater.*, 2013, **25**, 4497–4502.
56 S. A. Haque, E. Palomares, B. M. Cho, A. N. M. Green, N. Hirata, D. R. Klug and J. R. Durrant, *J. Am. Chem. Soc.*, 2005, **127**, 3456–3462.
57 T. D. Santos, A. Morandeira, S. Koops, A. J. Mozer, G. Tsekouras, Y. Dong, P. Wagner, G. Wallace, J. C. Earles, K. C. Gordon, D. Officer and J. R. Durrant, *J. Phys. Chem. C*, 2010, **114**, 3276–3279.
58 M. K. Nazeeruddin, A. Kay, I. Rodicio, R. Humphry-Baker, E. Muller, P. Liska, N. Vlachopoulos and M. Gratzel, *J. Am. Chem. Soc.*, 1993, **115**, 6382–6390.
59 J. Yang, D. K. Kersi, L. J. Giles, B. W. Stein, C. Feng, C. R. Tichnell, D. A. Schultz and M. L. Kirk, *Inorg. Chem.*, 2014, **53**, 4791–4793.